Pergamon

Int. J. Solids Structures Vol. 35, Nos 31–32, pp. 4205–4222, 1998

0020-7683/98 $19.00 + .00

PII: S0020-7683(97)0031-7

MICROMECHANICAL MODELING OF SOFTENING BEHAVIOR IN STEEL FIBER REINFORCED CEMENTITIOUS COMPOSITES

CHRISTOPHER K. Y. LEUNG*
Department of Civil and Environmental Engineering, MIT, Cambridge MA 02139, U.S.A.

and

Y. PHILIP GENG
Advanced Research Laboratory, IJBU, Hewlett-Packard Company, Corvallis OR 97330, U.S.A.

(*Received* 18 *October* 1996; *in revised form* 1 *June* 1997)

Abstract—The fracture of cementitious materials is governed by its softening behavior. When steel fibers are incorporated into concrete to improve its toughness, the softening behavior can be predicted in terms of the composite micro-parameters including the properties of fiber, matrix and interface as well as fiber size, length, distribution and volume fraction. In this paper, the bridging force provided by a steel fiber at any arbitrary angle to the crack is first modeled in terms of the micro-parameters. For a given fiber distribution, the averaged crack bridging force is then derived and employed to obtain the composite softening behavior. The model is verified at both the microscopic and macroscopic levels with experimental results from the fiber pull-out test and the four-point beam bending test. With the model, numerical simulations are carried out to study the effect of various parameters on the tensile softening behavior. These simulations can facilitate the choice of micro-parameters for the most cost-effective material design. © 1998 Published by Elsevier Science Ltd. All rights reserved.

INTRODUCTION

Cementitious materials fail through the propagation of cracks. Despite the incorporation of steel reinforcements, many common types of failure, such as diagonal shear in deep beams, punching shear in slabs, torsion of beams and pull-out of steel bars, still occur in a brittle manner (Bazant, 1992a). Associated with brittleness is the well-known size effect—a reduction in equivalent material strength with increasing size (Bazant, 1986). To avoid catastrophic failure and to incorporate the size effect into concrete design, the analysis of fracture processes in concrete has become a very important issue.

In recent years, significant advancements have been made in numerical techniques for the modeling of crack propagation in concrete and other quasi-brittle materials. These are summarized in various publications including Elfgren (1989), Gerstle and Bazant (1992), Bazant (1992b) and Bazant *et al.* (1994). Cracking in quasi-brittle materials are governed by the bridging stresses at the crack face, which is directly related to the tensile softening relation of the material. The softening relation is often obtained directly through tensile testing in a rigid frame (Peterson, 1981) or under close-loop control (Gopalaratnam and Shah, 1985a; Li and Shah, 1994). Alternatively, it can be derived indirectly from a J-based fracture testing scheme (Li *et al.*, 1985; Leung and Li, 1987).

When fibers are added to concrete in small volumes, the tensile strength is only slightly affected. However, post-peak tensile softening occurs much slower, implying significantly higher resistance to crack growth and hence a reduced brittleness. The softening behavior of fiber reinforced concrete is affected by the composite micro-parameters including the properties of fiber, matrix and interface as well as the fiber size, length, distribution and volume fraction. Since adding fibers will also increase the material cost, it is highly desirable

* Author to whom correspondence should be addressed.

to find an optimal combination of micro-parameters for the best cost-performance. With a large number of micro-parameters that can vary, the determination of the optimal combination based on empirical testing is very costly and hence impractical. An alternative approach is to develop a theoretical model for the prediction of softening behavior from micro-parameters. Simulations can be carried out to identify combinations of micro-parameters for high cost-effectiveness. A small number of experiments can then be carried out within the "optimal range" to find the most cost-effective design.

The objective of the present paper is to develop a micromechanical model for the softening behavior of steel fiber reinforced concrete, which is the most widely used fiber reinforced cementitious composite in practice. The theoretical approach involves two major steps: (i) derivation of crack bridging force for a single fiber in terms of micro-parameters through the analysis of micromechanisms, (ii) derivation of complete tensile behavior (including pre-peak and post-peak) from the bridging force and a given fiber distribution. Since we are focusing on composites with small fiber volume fractions, fiber interaction effects are not considered. After the model is verified at both the microscopic and macroscopic levels with experimental results from the fiber pull-out test and the 4-point beam bending test, numerical simulations are carried out to study the effect of various parameters on the tensile softening behavior.

DERIVATION OF CRACK BRIDGING FORCE FOR A SINGLE FIBER

In most practical fiber reinforced cementitious composites, the fibers are distributed in a quasi-random manner and hence can generally intersect with a crack at any angle. Figure 1 shows a fiber lying at an angle to the crack. Crack opening will induce both pulling and bending on the fiber. The crack bridging force P can then be separated into two components: S, the debonding/pull-out component due to interfacial stresses along the fiber, and R, the bending component due to reactions perpendicular to the fiber. The debonding/pull-out component can be obtained from the analysis of fiber sliding along the interface. To find

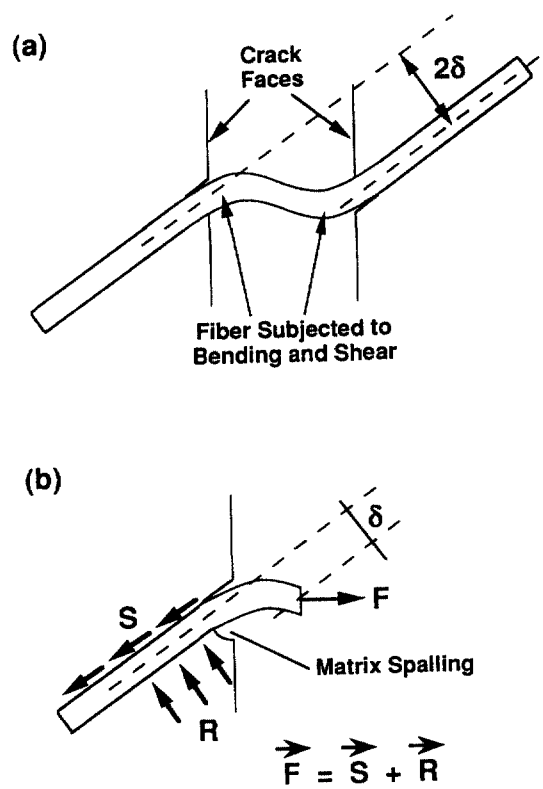

Fig. 1. (a) Bending of fiber across crack. (b) Components of crack bridging force.

the bending component, the fiber is treated as a beam bending on an elastic foundation with variable properties along its length. It should be noted that there is significant interaction between the two components of the bridging force. The post-yielding behavior of the steel fiber depends on the axial force along the fiber, which is related to fiber debonding/pull-out. On the other hand, the friction along the fiber interface, which governs fiber debonding/pull-out, is a function of the normal force on the interface arising from fiber bending. The modeling of matrix, fiber and interfacial behavior as well as their interactions are described in the following.

DERIVATION OF EQUIVALENT FOUNDATION PROPERTIES

As described above, fiber bending is modeled by treating the matrix as an elastic foundation. Determination of effective foundation properties was detailed in Leung and Li (1992). Here, only a brief account is provided. Let us consider a section of the composite cut in a direction perpendicular to the fiber (Fig. 2). The section is assumed to be under plane strain. In Fig. 2, h, the distance from the bottom of the fiber to the crack face, is a function of the distance x along the fiber. For fiber reinforced concrete, where the interfacial strength is weak, the interface is assumed to have debonded and under frictional contact in the region close to the crack face, where there is significant reaction stress. Load is applied to a horizontal line at the middle of the fiber cross section (Fig. 2). All points on the line are constrained to have the same vertical displacement. Under applied force F per unit length, the displacement u_f relative to the top of the plate (at distance H_1 from the fiber center, see Fig. 2) and the stress field around the fiber are computed to determine the foundation stiffness and spalling criterion. H_1, which affects the computed value of u_f, is chosen based on physical considerations detailed in Leung and Li (1992). The location of

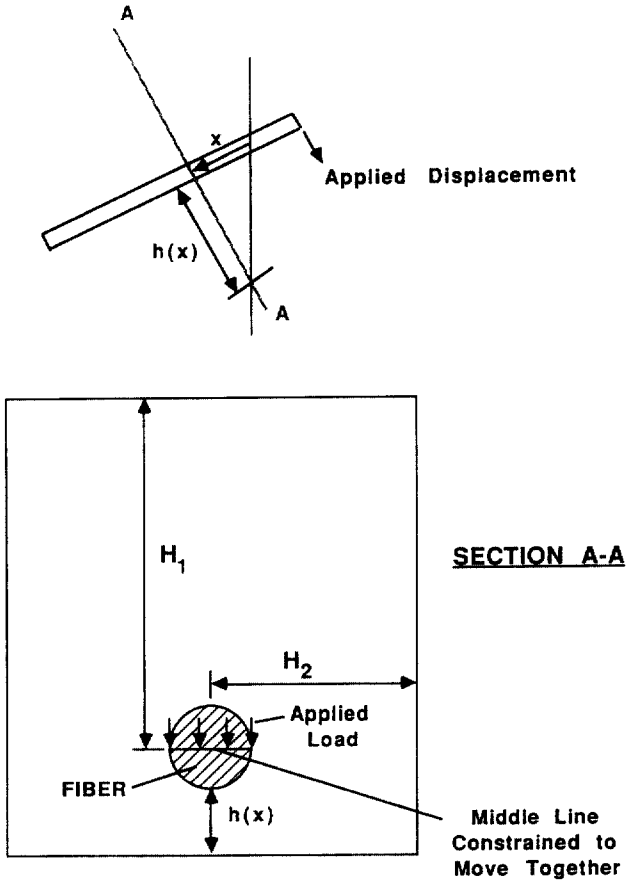

Fig. 2. Determination of equivalent foundation properties.

maximum principal stress in the plane of the cut section depends on the distance of fiber from the free surface. When h is small, maximum stress is found below the fiber. For large h, stress is maximum on the sides of the fiber near the two ends of the horizontal diameter. Once the maximum principal stress reaches the local strength of the material, matrix spalling will occur. When the fiber on an elastic matrix is bent at one end, it deflects downward at some points but upwards at other points. Therefore, foundation stiffness values have to be obtained for both cases with fiber pressing on the bottom or the top of its groove. Matrix spalling, on the other hand, always occurs around the bottom half of the fiber so the spalling criterion needs to be derived only for the case with the fiber pressing on the bottom of its groove.

To find the variation of foundation properties along the fiber, finite element analysis of the above 2-D contact problem was carried out. Foundation properties against h/r (where r is the fiber radius) for different moduli ratio is shown in Fig. 3. In the figures, $(k_m/E_m)_B$ and $(k_m/E_m)_T$ are, respectively, the normalized foundation stiffness when the fiber is pushing on the bottom and the top of its groove. $F_{sp}/\sigma_m r$ is the normalized applied force/unit length on the matrix when spalling occurs, with σ_m being the local matrix strength.

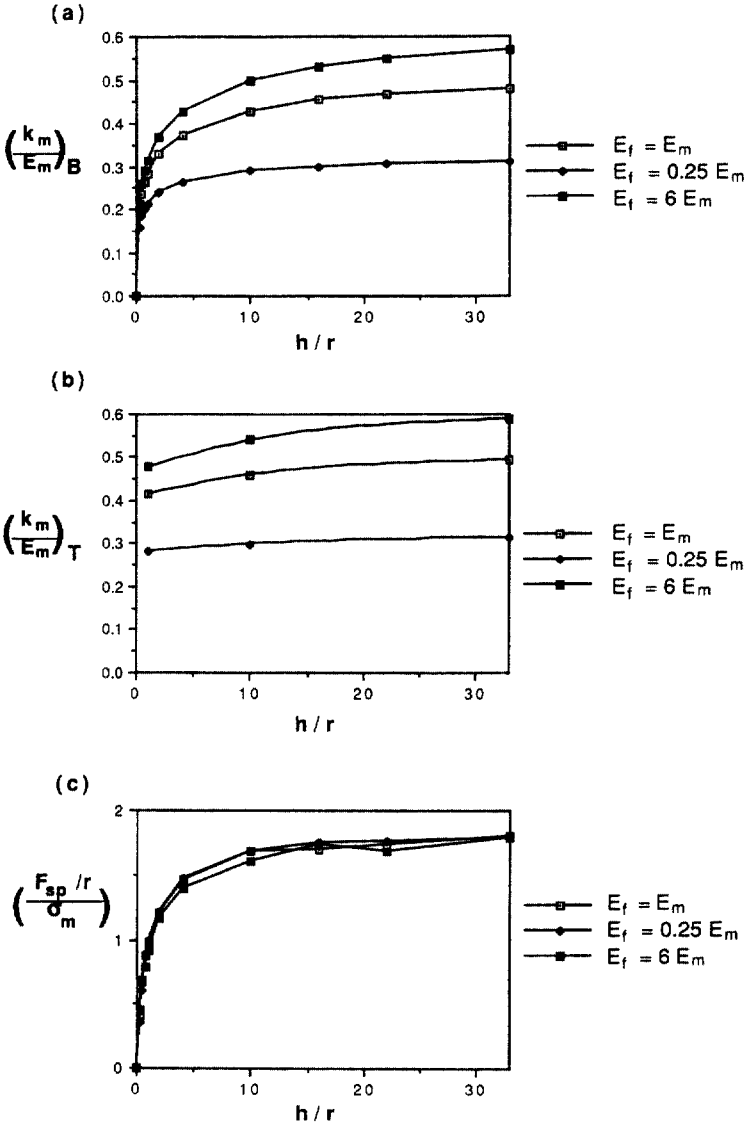

Fig. 3. Variation of foundation properties with h/r and E_f/E_m.

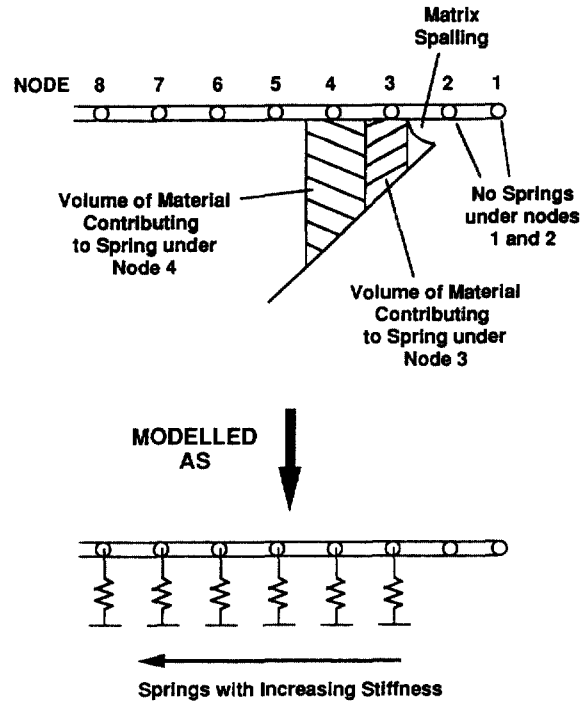

Fig. 4. Discretization of matrix into spring elements.

As expected, both the stiffness and spalling stress increase with h/r and approach asymptotic values when h/r becomes large.

Simulations (Leung and Li, 1992) have shown that the normalized foundation properties vs h/r curve shows little change for $E_f/E_m \geqslant 6$. For steel fiber reinforced concrete, E_f/E_m is higher than six, but the curves for $E_f/E_m = 6$ can be used. Physically, it means that when $E_f/E_m \geqslant 6$, the fiber can be considered rigid compared to the matrix.

To find the bridging force, the fiber is represented by beam elements. To model the matrix, the volume of unspalled material from the midpoint of one beam element to the midpoint of an adjacent beam element is represented by a discrete spring (Fig. 4) (Leung and Chi, 1995). The spring properties can thus be obtained as the integral of foundation properties from one midpoint to the next. Due to the sliding of fiber relative to the matrix, the foundation properties for a given node vary as crack opening increases. To correctly model the pull-out behavior, foundation properties are updated on each crack opening increment. For a node that has displaced out of the matrix by more than half the element size, the spring underneath is removed (nodes one and two in Fig. 4). To analyze the present problem, an alternative approach will be to keep the spring properties constant, but to re-mesh during the pull-out process to match the nodes of the beam elements to the location of the springs. This latter approach is not adopted, due to the difficulties in keeping track of loading history when partially yielded elements are re-meshed.

MODELING OF ELASTO-PLASTIC BENDING OF THE FIBER

When inclined steel fibers are pulled out of a cementitious matrix, yielding is commonly observed (Naaman and Shah, 1976; Leung and Shapiro, 1998). To model elasto-plastic fiber bending, several points have to be kept in mind. The elasto-plastic bending of fiber is affected by the axial tensile force arising from fiber stretching, which varies from point to point along the fiber. For any single point along the fiber, the axial force varies with crack opening. When the crack opens, the bridging force due to bending may decrease and any yielded parts of the fiber may be elastically unloaded.

Initial attempts to model the fiber with elasto-plastic iso-parametric elements are not successful due to the divergence of results for most cases. We therefore decided to simplify the analysis by using an approximate elasto-plastic beam element and an assumed loading history. The approach is briefly summarized below. Details can be found in Leung and Chi (1995).

To develop a simple beam element for elasto-plastic bending of the fiber, a unique moment–curvature (M–κ) relation is assumed to exist for a given axial force. Such a relation is obtained by first applying the axial force to the fiber cross-section and then determine the moment corresponding to a given curvature. The M–κ curves are then approximated by tri-linear relations. The first turning point of the curve occurs at a moment M_1 equal to the average of the yield moment and the ultimate moment. After the turning point, the slope of the second branch is reduced to one-fifth of the original. The third branch is a horizontal line (or one with a very small slope to facilitate numerical computation) which starts when the second branch reaches the ultimate moment. Such a tri-linear relation is found to well represent M–κ curves for a wide range of axial force (from 0–60% of the force for gross section yielding).

By replacing the exact M–κ with the tri-linear M–κ relation, a simple two-node elasto-plastic beam element can be developed as a direct extension of the linear elastic beam element. The slope reduction of the M–κ relation when it goes from one branch to another is represented by an equivalent change in Young's modulus of the material. Once the moment M_1 is reached at a certain node, modulus reduction (from initial value E_1 to $E_2 = E_1/5$) is assumed to occur over half an element length at each side of the node (Fig. 5). As shown in Fig. 5, for each element adjacent to the yielded node, half of it (the half closer to the yielded node) will have a reduced tangential modulus E_2 while the other half maintains the initial modulus E_1. The tangential stiffness matrix for such an element can be easily calculated in terms of E_1, E_2 and the element dimensions (see Leung and Chi, 1995). On further loading, yielding may occur on both nodes of the element. Then, the whole element will be "softened" to a reduced tangential modulus E_2.

To simplify the analysis, an assumption is also made on the loading history. Let us consider one-half of the fiber (Fig. 6(a)). For any increase in crack opening, the fiber should actually follow the path AB in the figure, during which the axial and bending forces on the fiber change simultaneously. To avoid dealing with such a complicated load history, we assume the fiber to displace in path ACDB in the figure, i.e., the fiber is assumed to be fully unloaded (A–C), displaced along its length (C–D) and then bent back to the curved configuration (D–B). If yielding has not started, the two histories will give the same results. After yielding, the assumed history is employed to simplify the analysis and its applicability is assessed by comparison with more accurate results (see below). With the assumed history, the elasto-plastic behavior at an element node under increasing crack opening is illustrated in Fig. 6(b). The node, originally following a M–κ curve for a given tensile load, is assumed to unload completely in bending (following the original elastic slope). After the axial load is changed, application of bending moment will cause the node to start yielding when an M–κ curve corresponding to the new axial load is reached. On subsequent bending, the new curve will be followed.

With the above assumptions, elasto-plastic bending of fiber on an elastic foundation is analyzed. Results are compared with those from the finite element program ADINA

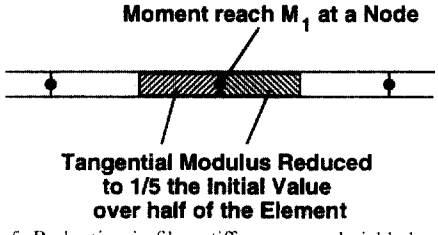

Fig. 5. Reduction in fiber stiffness around yielded node.

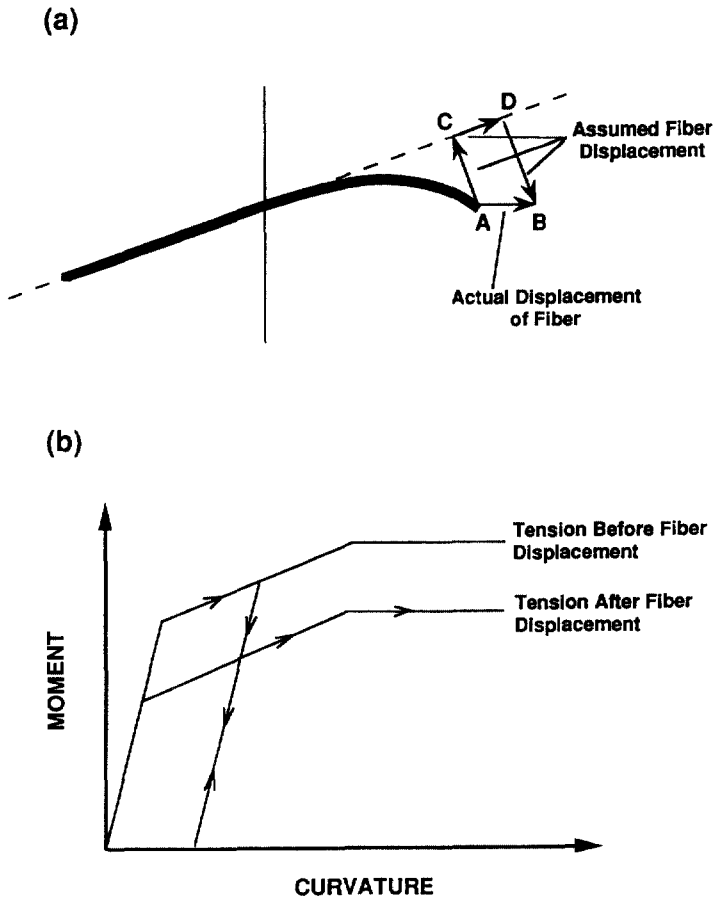

Fig. 6. (a) Actual and assumed displacement path as crack opening increases. (b) Assumed loading history at any yielded node.

using isoparametric elasto-plastic elements. Figure 7 shows the comparison for two cases where convergence in ADINA can be achieved to a reasonable degree. With different values of interfacial friction τ in the two cases, the axial stress distribution in the fiber and hence the yielding behavior are different. From the figure, very good agreement can be obtained up to the peak bridging force. In the post-peak regime, the prediction of the two models are still within 10%. Convergence can no longer be achieved in ADINA after a small post-peak displacement, while our model can calculate the continuous softening behavior. In the post-peak region where the largest difference in predictions can be observed, the prediction from ADINA may not be very reliable since it is on the verge of divergence. Besides the advantage in terms of convergence, the approximate approach we developed is also computationally far more efficient.

MODELING OF INTERFACIAL BEHAVIOR

Debonding and pull-out of steel fiber from a cementitious matrix have been analyzed by many investigators in the literature (Gopalaratnam and Shah, 1995; Gao *et al.*, 1988; Stang *et al.*, 1990; Naaman *et al.*, 1991; Leung and Geng, 1995) using both strength-based and energy-based approaches. In the present work, for simplicity, the interface is taken to be purely frictional. This assumption is acceptable for steel fibers, which do not bond strongly with concrete. In the pre-peak region, a constant interfacial friction can be assumed. Once debonding is completed, the decrease of interfacial friction with further sliding can be described by (Naaman *et al.*, 1991):

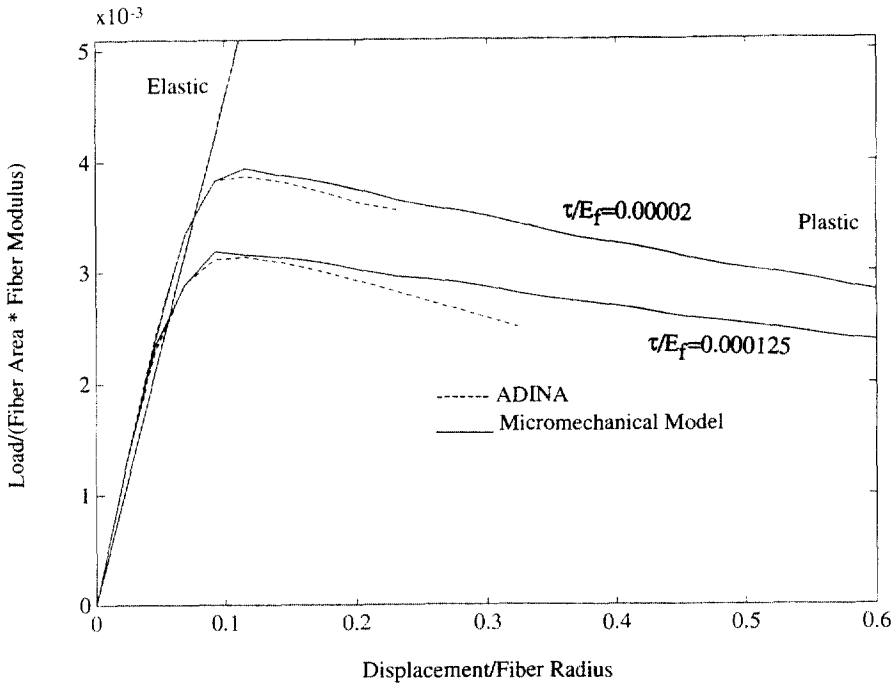

Fig. 7. Comparison of results between approximated approach and ADINA.

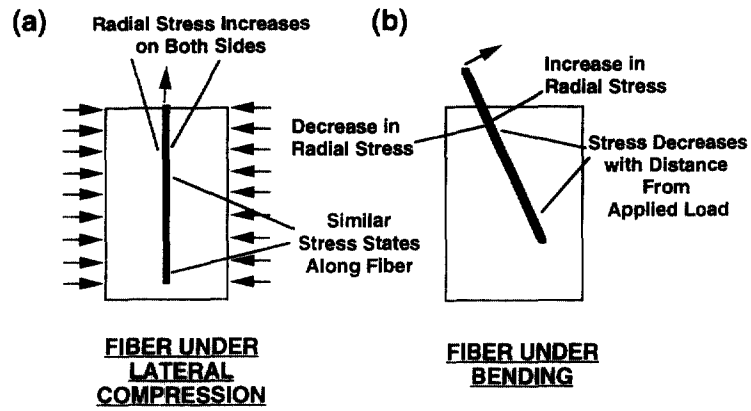

Fig. 8. Increase of radial stress for fiber under. (a) Uniform lateral compression. and (b) bending.

$$\tau_{i0}(s) = \tau_{i0}(0)\frac{\exp[-s^{\eta}] - \xi\exp[-L^{\eta}]}{1 - \xi\exp[-(L-s)^{\eta}]} \tag{1}$$

where s is the sliding distance after complete debonding, and ξ, η are parameters determined from data fitting. In eqn (1), the Poisson's effect has been neglected since it is considered minor compared to other effects.

When the fiber is bent onto the matrix (as shown in Fig. 1), the matrix reaction force can affect the frictional resistance of the interface. Due to the 3-D nature of the problem, the actual interaction is very complicated. In this work, we assume that the interfacial behavior during the pull-out of the bent fiber is similar to that in a fiber pulled out under uniform applied lateral stress. The latter problem has been studied in detail by Leung and Geng (1995) and Geng and Leung (1997). The similarities and differences of the two situations are illustrated in Fig. 8. In the following, we will briefly present an interfacial damage model for pull-out under applied lateral stress. (Note: for full details, please refer

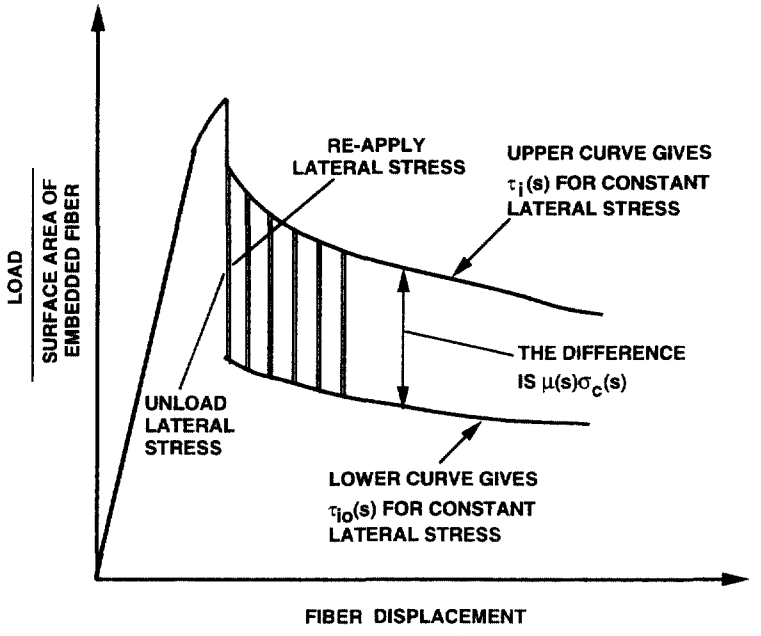

Fig. 9. Schematic showing the decomposition of friction into two components.

to Geng and Leung, 1997). Empirical modification of the damage model for the bent fiber will then be discussed.

Leung and Geng (1995) has shown that the presence of lateral force can significantly affect the fiber debonding/pull-out behavior. To account for such an effect, the interfacial friction is decomposed into two components, τ_{i0} and $\mu\sigma_c$. τ_{i0} is the residual friction of the interface (when there is no lateral stress acting), μ the frictional coefficient and σ_c the equivalent lateral stress. An experimental approach to obtain τ_{i0} and $\mu\sigma_c$ separately is illustrated in Fig. 9. Fiber pull-out test is carried out under lateral compression, with a biaxial loading set-up (Leung and Geng, 1995; Geng and Leung, 1997). During the pull-out test, the lateral compression is unloaded and re-applied for a number of times. The curve formed by points after unloading represents the variation of τ_{i0} with sliding distance (s) for the given lateral compression. The difference between the upper and lower curves allows the calculation of μ as a function of s. Experiments have been carried out with different values of lateral compression and the results are reported in Geng and Leung (1997). Here, the major findings from the experiments are summarized.

For a given sliding distance s, values of both τ_{i0} and μ can be obtained as described above. Plotting τ_{i0} and μ against one another shows that the data for all different combinations of sliding distance and lateral compression history appears to follow the same line. Physically, this may be explained by the fact that both parameters are dependent on the current status of the interface and a one-to-one correspondence therefore exists. Based on the experimental results, an empirical relation between μ and τ_{i0} can be obtained:

$$\mu = 0.08 + (\tau_{i0}/21.28) \tag{2}$$

where τ_{i0} should be in MPa.

The above finding has important implications. Since μ is a function of τ_{i0}, if $\tau_{i0}(s)$ can be found, the total interfacial resistance can be obtained for a given lateral compression σ_c. To find τ_{i0}, we assume that the damage (or smoothening) rate of the interface is a function of its current state as well as the current lateral compression. In equation form, it is given by:

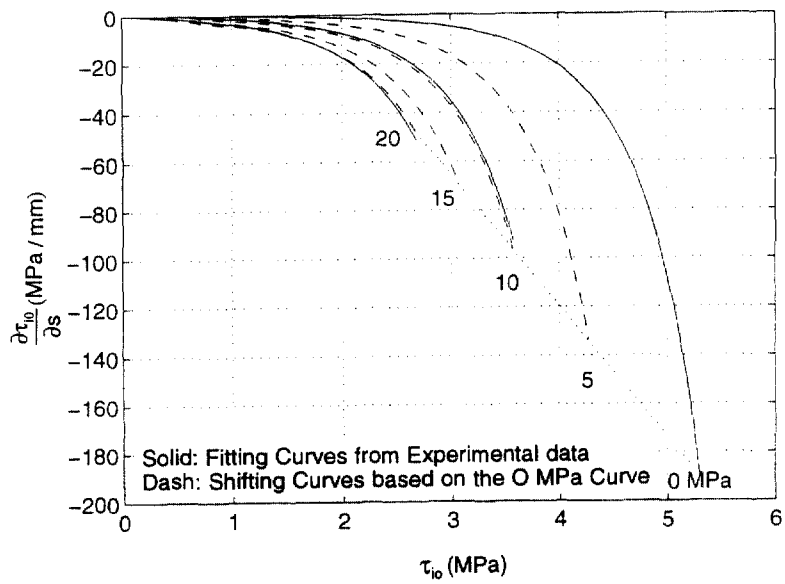

Fig. 10. Shifting of $\partial\tau_{i0}/\partial s$ vs τ_{i0} curves for different compression levels.

$$\partial\tau_{i0}/\partial s = F(\tau_{i0}, \sigma_c) \tag{3}$$

Based on experimental results obtained as in Fig. 9, τ_{i0} vs s is first fitted with a polynomial. $\partial\tau_{i0}/\partial s$ is then plotted against τ_{i0} for different values of σ_c. The results are shown in Fig. 10 as solid lines. An interesting observation is that the curves for higher lateral compression appear to be part of the $\sigma_c = 0$ curve, but shifted horizontally. Also, the starting point of the curves for different σ_c values appear to lie on a straight line. The dashed curves in Fig. 10 are obtained by horizontally shifting the $\sigma_c = 0$ curve, with the starting point of each curve lying on a straight line. The good agreement between the shifted and experimentally derived results (dashed and solid curves, respectively) justify the use of a simple shifting scheme to obtain $\partial\tau_{i0}/\partial s$ vs τ_{i0} curves for intermediate σ_c values.

With $\partial\tau_{i0}/\partial s$ expressed in terms of τ_{i0} and σ_c, $\tau_{i0}(s)$ after any lateral loading history can be calculated from:

$$\tau_{i0}(s)|_{\sigma_c(s)} = \tau_{i0}(0)|_{\sigma_c(0)} + \int_0^s \frac{\partial\tau_{i0}}{\partial\zeta}\Big|_{\sigma_c(\zeta),\tau_{i0}(\zeta)} \mathrm{d}\zeta \tag{4}$$

The above results are obtained for the case with lateral compression on both sides of a fiber. Also, although the compression may change in magnitude, it stays uniform along the fiber length. For the bent fiber considered in this paper, lateral stress is increased on the side with the fiber pushing onto the matrix but decrease on the other side. However, from equilibrium considerations, there would be a net increase in lateral stress (or radial stress) on the fiber interface. Since the bending component is small before the whole fiber starts to pull out, the effect of lateral stress is neglected before the fiber is fully debonded. During fiber pull-out, the effect of lateral stress is considered in an approximate manner by assuming an equivalent lateral compression σ_{ce} given by:

$$\sigma_{ce} = c(N/2r) \tag{5}$$

where N is the average reaction force per unit length acting on the fiber and r is the fiber radius. c is an empirical factor to be obtained from the pull-out test result. Note that σ_{ce} is assumed to be the same on every point of the fiber interface, and so every point along the interface will degrade to the same extent. This assumption significantly reduces the amount of computation required when each point on the interface is subject to different lateral

stress and degrade to different extents. The adequacy of the assumption can be assessed by comparing model prediction with experimental results, which will be described in the next section.

PREDICTION OF CRACK BRIDGING FORCE

With the modeling approach and assumptions described above, this section will provide a brief summary of the computational steps. Before one can compute the crack bridging behavior, the composite micro-parameters need to be known. The Young's moduli and yield strength of the steel fiber are usually supplied by the fiber manufacturer. For concrete, modulus can be found from standard cylinder test. The determination of spalling strength, σ_m, however, is not as straightforward. Being the strength of a very small amount of matrix material around the fiber, σ_m is much higher than the macroscopic tensile strength obtained from specimens with significantly larger flaws. Since it is not possible to measure σ_m directly, its value is obtained by fitting the experimental pull-out results. In other words, σ_m is a fitting parameter in the model, though it possesses a clear physical meaning. When spalling occurs, the matrix always break off in small chunks of a certain size. In other words, when the finite element model for the matrix is refined to provide more accurate stress and displacement results, the spalling size should be kept constant. If elements are smaller than the spalling size, several elements will spall together when the total force acting on them is greater than their total spalling resistance. In the model the spalling size is chosen to be 0.4 mm. This is within the range of size for small matrix pieces that crumble off during the experiment.

The interfacial parameters for steel fiber include the interfacial friction τ_i and all the other parameters in eqn (1) governing the softening rate of the interface. All these parameters are obtained by fitting eqn (1) to the experimental pull-out curves for 0° (i.e., pull-out curve for a fiber perpendicular to the crack surface). In the present research program, the same concrete composition and fiber are used in (i) the pull-out tests under lateral compression, based on which eqns (2)–(4) are derived, and (ii) pull-out tests on inclined fibers for the verification of the micromechanical model, which will be presented later. We therefore assume the relation between τ_{i0} and μ as well as the shifting scheme in Fig. 10 to hold for the inclined fiber pull-out tests. Then, c in eqn (4) is the only parameter not known. As discussed above, it is left as a fitting parameter in the model.

For the steel fiber, the Young's modulus is well known. The yield strength is supplied by the manufacturer, but can also be easily obtained in a standard tensile test with a wire testing fixture.

To compute fiber pull-out behavior, all the known material parameters, and stipulated values of σ_m and c, are input into the program. Also, the numerical values of normalized foundation properties in Fig. 2 need to be input. The first step of the analysis is then to relate the fiber displacements u_a and δ (in directions along the perpendicular to the fiber) to the crack opening. Also, the free length of fiber (l_f) beyond the matrix foundation needs to be found. An approach first proposed by Morton and Groves (1974) is employed. The fiber is separated into two free bodies at the middle of the crack where the point of inflection is located (Fig. 11). Based on simple geometry and trigonometry, u_a, δ and l_f can be expressed in terms of the half crack opening, u, and the fiber radius, r, as:

$$u_a = u\cos\theta \tag{5}$$

$$\delta = u\sin\theta \tag{6}$$

$$l_f = r\tan\theta + u\cos\theta \tag{7}$$

where θ is the angle between the fiber and the normal to the crack plane. In the expression for l_f, the first term is contributed by the part of fiber separated from the matrix on bending (Fig. 11) and the second term is due to displacement of fiber into the crack (i.e., u_a).

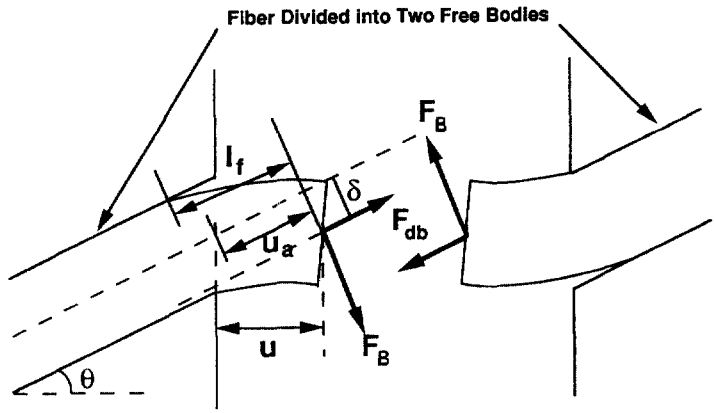

Fig. 11. Configuration for determination of crack bridging force due to debonding, pull-out and bending.

With u_a known, the debonding/pull-out component F_{db} can be computed. Before the whole fiber is debonded, a constant friction τ_i is assumed. F_{db} is then related to u_a through:

$$F_{db} = [4\pi^2 r^3 \tau_i u_a (1 + E_f V_f / E_m V_m)]^{1/2} \tag{8}$$

When debonding of the fiber is completed (i.e., fiber pull-out is just about to start), the initial residual friction is given by:

$$\tau_{i0}(0) = \tau_i - \mu(0)\sigma_{cc} \tag{9}$$

where σ_{cc} can be obtained from the reaction force as a result of fiber bending. Since $\tau_{i0}(0)$ and $\mu(0)$ are linearly related to one another, eqn (9) allows the determination of $\tau_{i0}(0)$.

During fiber pull-out, $\tau_{i0}(s)$ is obtained from eqn (3). At each step, the additional change in $\tau_{i0}(s)$ is computed based on the σ_{cc} value at the end of the previous step. Knowing the relation between $\tau_{i0}(s)$ and $\mu(s)$, the total interfacial friction $\tau_i(s)$ can be easily obtained. The pull-out force F_{db} is the product of $\tau_i(s)$ and the remaining embedded surface area of the fiber.

Once $\tau_i(s)$ and F_{db} are known, the axial force at any node along the fiber can be calculated. The appropriate M–κ relation can then be prescribed. The bending force F_B required to produce a lateral displacement δ for a free length l_f of fiber can then be found. At each step, for computational convenience, the fiber is assumed to unload in bending, pulled along its length and bent again. The residual displacement and moments along the fiber therefore needs to be documented. Due to the elastic unloading assumption, the bending analysis at each step always starts with an elastic beam. In the computational algorithm, displacement is applied to the beam until yielding occurs at a particular point of the beam or the matrix foundation spalls. The global stiffness is then updated. Further displacement is applied until the occurrence of the next yielding or spalling, when the stiffness is again updated. The process is repeated until the required displacement is reached at a force F_B. Knowing both F_{db} and F_B, the total bridging force is calculated as the sum of their components along the crack opening direction.

In Fig. 12, pull-out curves obtained from the model are compared with experimental results on steel fiber pulled out at 0, 30 and 60 . The three plots on the left hand side are the experimental results while the right hand side shows the theoretical prediction together with one representative experimental curve for each case. In the model, σ_m and c are taken to be 150 MPa and 0.2, respectively. In the experiment, the compliance of fixtures greatly increase the measured displacement. The model results have therefore been corrected by adding to the displacement a value $u_{corr} = kP$, where P is the total bridging force. The value of k is obtained from the peak displacement and load values for the 0 case. Based on Fig.

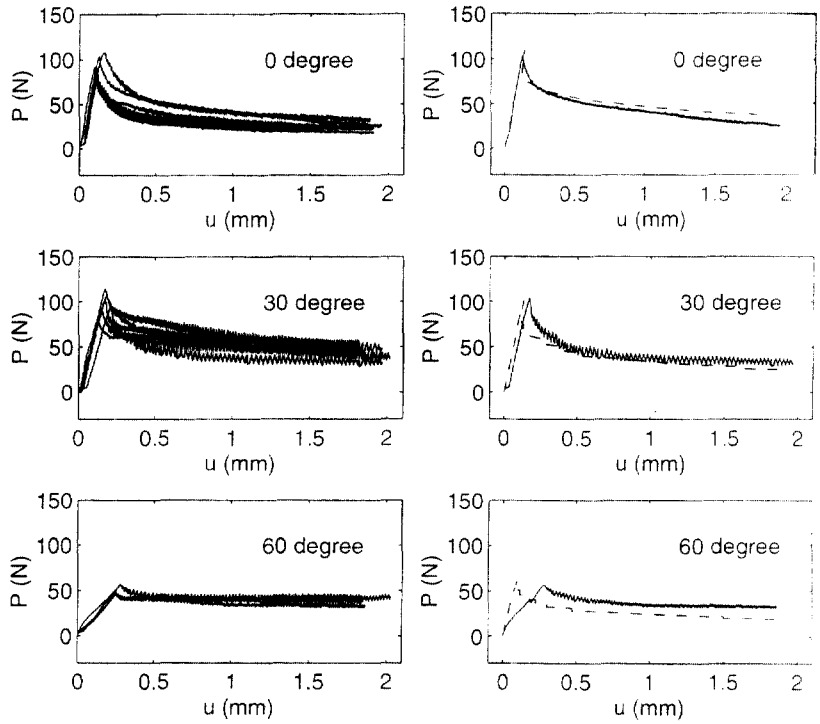

Fig. 12. Experimental pull-out curves (left) and model predictions (right, dash line).

12, one can see that the present model can correctly predict both the peak pull-out load and the post-peak softening behavior for different inclination angles. This is a significant improvement over previous models (Li *et al.*, 1990; Ouyang *et al.*, 1994) which, despite the use of fitting parameters, can only predict the peak pull-out load.

DERIVATION OF SOFTENING BEHAVIOR OF FIBER REINFORCED CONCRETE

To derive the complete tensile behavior, the first step is to calculate the averaged bridging force provided by all the fibers. Assuming low volume fraction, the interaction effects between closely spaced fibers can be neglected. In this paper, we assume a 2-D random fiber distribution. Let's define L as the embedded length of the fiber when the crack opening is zero. Since fiber pull-out always occurs at the shorter side, L will be uniformly distributed between 0 and $L_f/2$ for all the fibers bridging the crack. The probability density function of L is then given by $p(L) = 2/L_f$. Also, if the angle θ is uniformly distributed from 0 to $\pi/2$, the probability density function $p(\theta)$ is equal to $(2/\pi)\cos\theta$ (Aveston and Kelly, 1973; Li *et al.*, 1991). The average bridging force for all fibers is then given by:

$$F(u) = \int_{\theta=0}^{\pi/2} \left\{ \int_{L=0}^{L_f/2} P(L, \theta, u) p(L)\, \mathrm{d}L \right\} p(\theta)\, \mathrm{d}\theta \tag{10}$$

where $P(L, \theta, u)$ is the pull-out force at the given u for a fiber with original embedded length L and inclination θ.

With the model for bridging force developed above, $P(L, \theta, u)$ can be computed. To illustrate the computation of averaged bridging force, the fiber length is taken to be 20 mm. The initial embedded length can hence range from 0 to 10 mm. To numerically evaluate the double integral in eqn (10), 10 discrete values of L (1 mm apart) and 18 values of θ (5° apart) are employed. Then, for a composite with volume fraction V_f, the averaged crack bridging stress σ_B given by:

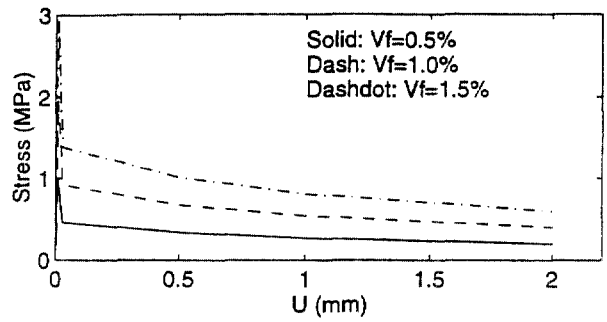

Fig. 13. Bridging stress vs crack opening for three fiber volume fractions.

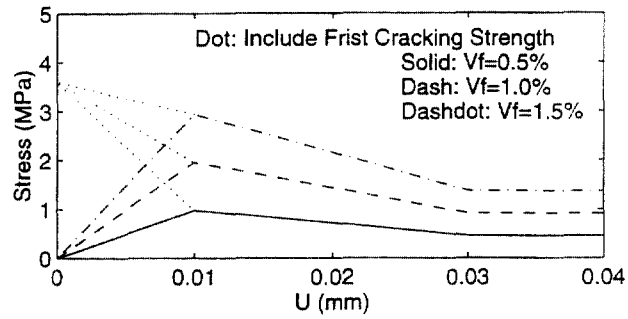

Fig. 14. Softening behavior for three fiber volume fractions.

$$\sigma_B(u) = V_f F(u)/\pi r^2 \tag{11}$$

The result of averaged crack bridging stress for $V_f = 0.5$, 1.0 and 1.5% are shown in Fig. 13. The corresponding softening behavior is shown in Fig. 14. For small volume fraction, the tensile strength of the concrete is assumed to stay the same. After cracking, the stress is assumed to drop from the tensile strength to the value corresponding to the peak fiber bridging stress (see dotted lines in Fig. 14). Note that this modeling approach is only valid for small V_f, when the maximum bridging stress is lower than the matrix tensile strength. Otherwise, multiple cracking will occur and the tensile behavior will have a pseudo-ductile branch before the peak is reached. This pseudo-ductile case is preferable but is not easy to be achieved with low cost fibers and conventional casting techniques.

To assess the validity of the derived softening behavior, it is implemented into a computational framework. The predicted behavior of a beam in four-point bending is then compared with experimental results. In the analysis, the uncracked part of the member is represented by eight node quadratic elements and the bridging force in the crack is modeled by a bar element with a force vs displacement relation corresponding to the softening relation in Fig. 14. Note that the discrete cracking approach employed here is only applicable when the crack location and direction are both known beforehand. Otherwise, a smeared cracking approach would be required.

Four point bending tests are carried out with fiber reinforced mortar beams of 457.2 mm (length) × 114.3 mm (depth) × 76.2 mm (width). With 20 mm fibers, three fiber volume fractions (0.5, 1.0 and 1.5%) are employed. The mortar composition (w/c/s = 0.5 : 1 : 2) is the same as that employed in the fiber pull-out test. In the specimen preparation, the mold is filled and vibrated in several layers to produce an approximately 2-D random fiber distribution. The experimental results, in terms of applied load vs mid-span displacement, are shown as broken lines in Fig. 15. The solid line in the figure are the results from finite element analysis. Note that the experimental results exhibit a significantly higher pre-peak displacement than the model predictions. This may be due to the initial seating of the beam

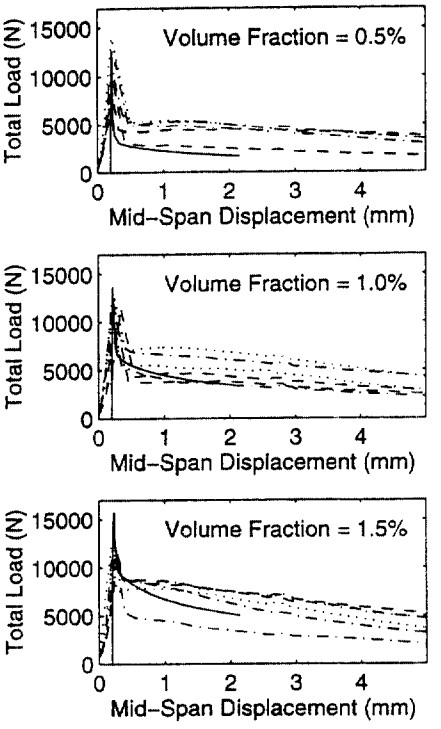

Fig. 15. Model prediction of four point beam bending behavior (solid line) and experimental results (other lines).

as well as local deformation at the supports. The peak load as well as the post-peak behavior are, however, in good agreement with experimental results.

PARAMETRIC STUDIES

The agreement of experimental results and model predictions in Fig. 15 supports the validity of the micromechanical modeling approach. The actual power of the approach, however, lies in the ability to study the effects of various parameters on the softening behavior. As illustrations of this important point, averaged bridging force are computed for various combinations of micro-parameters. The results are shown in Figs 16–18. Note that for small volume fractions, the softening behavior is directly related to the averaged bridging force [refer to eqn (11) and Fig. 14]. The trend of averaged bridging force is therefore a direct indication of the trend of the softening behavior.

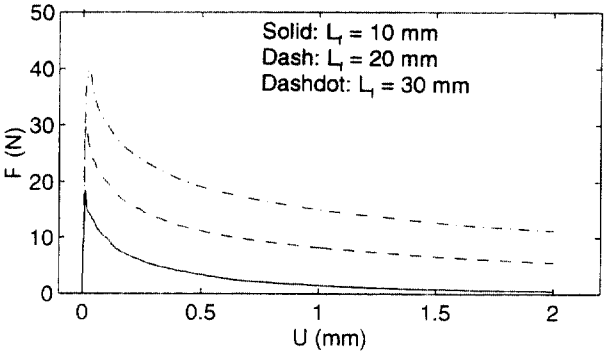

Fig. 16. Effect of fiber length on averaged fiber bridging force.

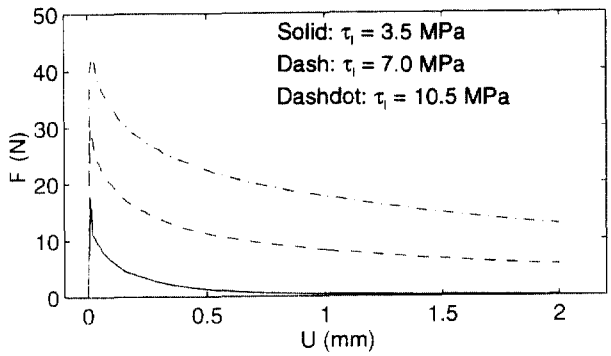

Fig. 17. Effect of interfacial friction on averaged fiber bridging force.

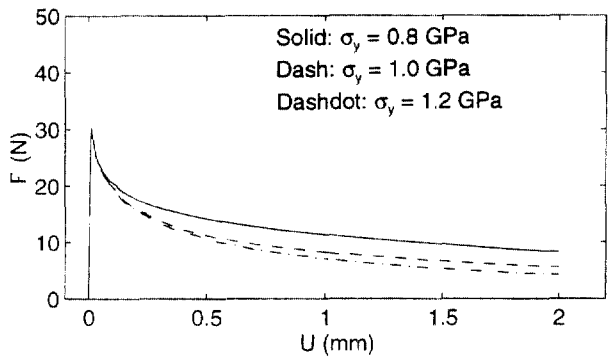

Fig. 18. Effect of fiber yield strength on averaged fiber bridging force.

Figures 16 and 17 show, respectively, the effects of fiber length and interfacial friction. The middle curve in both plots are the same. As expected, a longer length or higher interfacial friction leads to higher averaged bridging force. An interesting observation is that increasing the interfacial friction by 50% (relative to the middle curve) gives roughly the same effect as increasing the fiber length by 50%. Close comparison of the curves reveals that a 50% increase in friction actually gives rise to a higher F–u curve than a 50% increase in length. Since increasing the fiber length may also lead to workability problems, the simulation indicates that within the range of micro-parameters being studied, roughening the fiber surface (to increase the friction) is the better way to improve composite behavior than increasing the fiber length.

Figure 18 shows the effect of varying the fiber yield strength. By increasing the yield strength from 0.8–1.2 GPa, the bridging force reaches about the same peak but drop much faster with increasing fiber yield strength. The pull-out work (or energy absorption during the pull-out process), which is given by the total area below the F–u curve, therefore decreases with fiber yield strength. This interesting observation can be explained as follows. In a random fiber composite, most fibers are lying at an angle to the crack. As the crack opens, fiber bending (as illustrated in Fig. 1) can lead to matrix spalling. With a higher fiber yield strength, more matrix spalling can occur, leading to a more rapid decrease in pull-out resistance. The simulated results are consistent with pull-out test results by Leung and Shapiro (1998) (Fig. 19). In the tests, fibers of different yield strength are embedded at different angles in the pull-out specimens. For each pull-out result, the pull-out work is calculated from the total area under the experimental curve. Because the fibers with different yield strength also exhibit different pull-out behavior at zero degree, the pull-out work for the zero degree case is subtracted from the inclined fiber cases. The net pull-out work is called the bending component, which reflects the effect of yield strength if all the fibers have the same interfacial behavior. From the bending component of pull-out work shown in Fig. 19, it is clear that an optimal yield strength (for maximum pull-out work) exists

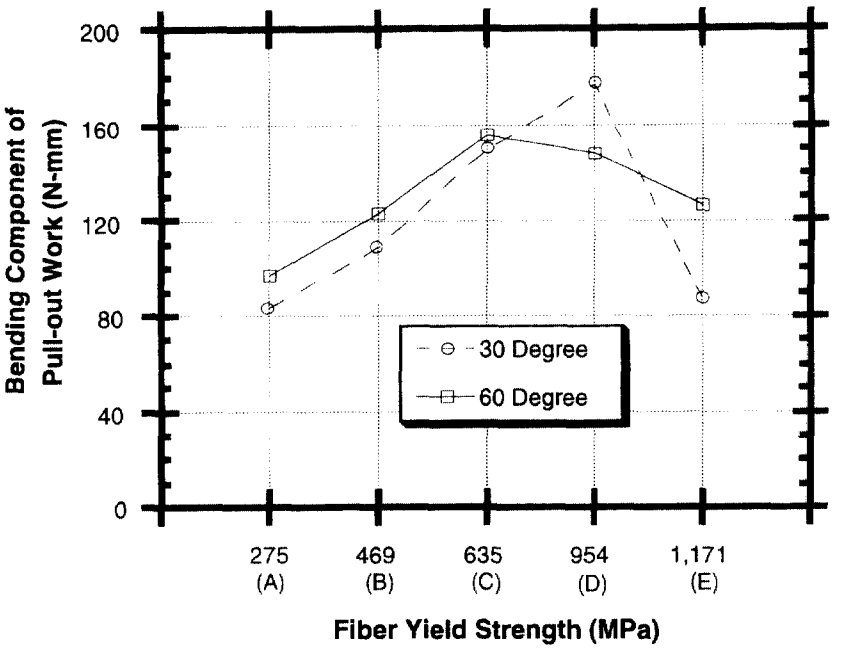

Fig. 19. Effect of fiber yield strength on bending component for fiber pull-out work.

between 0.635 and 0.954 GPa. Increasing the yield strength from 0.8–1.2 GPa, as in the simulation, should therefore result in a decrease in pull-out work.

CONCLUSION

In the present work, a micromechanical model is developed to derive the softening behavior of fiber reinforced cementitious composites. A key step in the model, the derivation of crack bridging force for a single fiber, is verified by fiber pull-out test results. The derived softening behavior is implemented into a numerical framework for the prediction of component behavior. Good agreement between model prediction of beam bending behavior and experimental results provide further support to the validity of the micromechanical modeling approach. With the micromechanical model, parametric studies of softening behavior are carried out. Within the range of parameters being studied, it is found that, increasing the interfacial friction is a better alternative to improving material behavior than increasing fiber length. Also, beyond a certain point, increasing the fiber yield strength is not desirable. The simulation results demonstrate the potential of micromechanical models as a useful tool in material development and design.

REFERENCES

Aveston, J. and Kelly, A. (1972) Theory of multiple fracture of fibrous composites. *Journal of Materials Science* **8**, 352–362.

Bazant, Z. P. (1986) Mechanics of distributed cracking. *ASME Applied Mechanics Review* **39**(5), 675–705.

Bazant, Z. P. (1992a) Should design codes consider fracture mechanics size effect. In *Concrete Design Based on Fracture Mechanics*, ACI SP-134, ed. W. Gerstle and Z. P. Bazant, pp. 1–23.

Bazant, Z. P. (1992b), ed. *Fracture Mechanics of Concrete*. Elsevier, London.

Bazant, Z. P., Bittner, Z., Jirasek, M. and Mazars, J. (1994), ed. *Fracture and Damage in Quasibrittle Structures: Experiment, Modeling and Computer Analysis*. E&FN Spon, London.

Elfgren, L. (1989), ed. *Fracture Mechanics of Concrete Structures—from Theory to Applications*. Chapman and Hall, London.

Gao, Y., Mai, Y. W. and Cotterell, B. (1988) Fracture of fiber reinforced materials. *ZAMP* **39**(4), 550–572.

Geng, Y. P. and Leung, C. K. Y. (1997) Damage-based modeling of fiber pull-out under variable lateral compressive stress. *ASCE J. Eng. Mech.* **123**(4), 342–349.

Gerstle, W. and Bazant, Z. P. (1992), ed. *Concrete Design Based on Fracture Mechanics*. ACI SP-134.

Gopalaratnam, V. S. and Shah, S. P. (1985a) Softening response of plain concrete in direct tension. *ACI Journal* **82**(3), 310–330.

Gopalaratnam, V. S. and Shah, S. P. (1985b) Tensile failure of steel fiber-reinforced mortar. *ASCE J. Eng. Mech.* **113**(5), 635–652.

Leung, C. K. Y. and Chi, J. (1995) Derivation of crack bridging force in random discontinuous fiber composites through micromechanics. *ASCE J. Eng. Mech.* **121**(12), 1315–1324.

Leung, C. K. Y. and Geng, Y. (1995) Effect of lateral stresses on fiber debonding and pullout. *Comp. Engrg* **5**(10–11), 1331–1348.

Leung, C. K. Y. and Li, V. C. (1989) Determination of fracture toughness parameter of quasi-brittle materials with laboratory-size specimens. *Journal of Materials Science* **24,** 854–862.

Leung, C. K. Y. and Li, V. C. (1992) Effect of fiber inclination on crack bridging stress in brittle fiber reinforced brittle matrix composites. *Journal of Mechanics and Physics of Solids* **40**(6), 1333–1362.

Leung, C. K. Y. and Shapiro, N. (1998) Optimal steel fiber strength for the reinforcement of cementitious materials. *ASCE J. Mat. Civ. Eng.*, accepted.

Li, Z. and Shah, S. P. (1994) Localization of microcracking in concrete under uniaxial tension. *ACI Materials Journal* **91**(4), 372–381.

Li, V. C., Wang, Y. and Backer, S. (1990) Effect of inclining angle, bundling and surface treatment on synthetic fiber pull-out from a cement matrix. *Composites* **21**(2), 132–140.

Li, V. C., Wang, Y. and Backer, S. (1991) A micromechanical model of tension-softening and bridging toughening of short fiber reinforced brittle matrix composites. *Journal of Mechanics and Physics of Solids* **39**(5), 607–625.

Li, V. C., Chan, C. M. and Leung, C. K. Y. (1987) Experimental determination of the tension-softening relations for cementitious composites. *Cement and Concrete Research* **17**(4), 441–452.

Morton, J. and Groves, G. W. (1974) The cracking of composites consisting of discontinuous ductile fibers in a brittle matrix—effect of fiber orientation. *Journal of Materials Science* **9,** 1436–1445.

Naaman, A. E. and Shah, S. P. (1976) Pull-out mechanism in steel fiber reinforced concrete. *ASCE J. Struct. Div.* **102**(8), 1537–1548.

Naaman, A. E., Namur, G. G., Alwan, J. M. and Najm, H. S. (1991) Fiber pullout and bond slip. I: Analytical study. *ASCE Journal of Structural Engineering* **117**(9), 2769–2790.

Ouyang, C., Alvarez, A. P. and Shah, S. P. (1994) Pull-out of aligned and inclined fibers from cement-based matrices. *ASCE Journal of Engineering Mechanics* **120**(12), 2641–2659.

Petersson, P. E. (1981) Crack growth and development of fracture zones in plain concrete and similar materials. Report TVBM-1006, Lund Institute of Technology, Division of Building Materials.

Stang, H., Li, Z. and Shah, S. P. (1990) The pull-out problem—the stress vs fracture mechanics approach. *ASCE J. Eng. Mech.* **116**(10), 2136–2150.